Atmospheric Research 157 (2015) 56–65

Contents lists available at ScienceDirect

Atmospheric Research

journal homepage: www.elsevier.com/locate/atmos

Column-integrated aerosol optical properties and direct radiative forcing based on sun photometer measurements at a semi-arid rural site in Northeast China

Yunfei Wu [a,b,*], Jun Zhu [c], Huizheng Che [d], Xiangao Xia [c], Renjian Zhang [a,*]

[a] Key Laboratory of Regional Climate-Environment for Temperate East Asia, Institute of Atmospheric Physics, Chinese Academy of Sciences, Beijing 100029, China
[b] State Key Laboratory of Loess and Quaternary Geology, Institute of Earth Environment, Chinese Academy of Sciences, Xi'an 710075, China
[c] Key Laboratory of Middle Atmosphere and Global Environment Observation, Institute of Atmospheric Physics, Chinese Academy of Sciences, Beijing 100029, China
[d] Key Laboratory for Atmospheric Chemistry, Center for Atmosphere Watch and Services, Chinese Academy of Meteorological Sciences, CMA, Beijing 100081, China

ARTICLE INFO

Article history:
Received 15 November 2014
Received in revised form 21 January 2015
Accepted 22 January 2015
Available online 31 January 2015

Keywords:
Semi-arid
Aerosol optical properties
Radiative forcing

ABSTRACT

Ground and satellite remote sensing measurements have revealed heavy aerosol loading in China; however, aerosol optical properties and direct radiative forcing in Northeast China – important in climate modeling and remote sensing – have not been widely studied. We studied four years of continuous sun photometer measurements at Tongyu, a typical semi-arid rural site in Northeast China, to better understand column-integrated aerosol optical properties and direct radiative forcing. The annual average aerosol optical depth (AOD) at 500 nm was 0.20 ± 0.26; the Ångström exponent (AE) between 440 and 870 nm was 1.37 ± 0.64; and the single scattering albedo (SSA) at 440 nm was 0.91 ± 0.05. The AOD at this rural site was a quarter of that observed in the polluted North China Plain and Yangtze River Delta regions. Anthropogenic fine-mode particles were the dominant contributor to AOD. The AOD and AE showed generally opposite seasonal variation patterns. Relatively higher AOD values in summer (0.26 ± 0.27) and spring (0.24 ± 0.30) were likely related to long-range transportation of anthropogenic aerosols from southern industrial regions in summer, and the increased contribution of dust events in spring. The minimum AOD (0.16 ± 0.22) was concurrent with the maximum AE (1.75 ± 0.76), observed in winter. On average, the absorption AOD (AAOD) at 440 nm and its absorption Ångström exponent (AAE) between 440 and 870 nm were 0.06 ± 0.03 and 1.04 ± 0.43, respectively. The mean AAE was considerably higher than 1 in autumn and winter, indicating that brown carbon from biomass burning contributed greatly to aerosol absorption. The AAE was lower than 1 in summer and spring, related to the coating of black carbon particles. Large negative aerosol direct radiative forcing was estimated at the bottom of the atmosphere, with relatively lower values estimated at the top of the atmosphere; the means were −26.28 and −9.42 W m^{-2}, respectively. This resulted in a strong cooling effect on the surface, but warming in the atmosphere, potentially impacting the regional climate.

1. Introduction

More than one third of China is covered by arid and semi-arid areas (Fu and An, 2002). The land–atmosphere processes in these regions play an important role in global and regional climate systems, like the East Asian Monsoon circulation (Liu et al., 2008). Changes in climate and climate variability impact the water and energy cycles in these regions (Huang et al., 2008). As a climatic and ecological transitional zone, investigation of semi-arid areas is key to understanding aridification, due to its high sensitivity and vulnerability (Fu and Wen, 2002).

* Corresponding authors.
E-mail addresses: wuyf@mail.iap.ac.cn (Y. Wu), zrj@mail.iap.ac.cn (R. Zhang).

http://dx.doi.org/10.1016/j.atmosres.2015.01.021
0169-8095/

To further investigate land–atmosphere processes and climate change in semi-arid regions, and the role of human activities, the Tongyu observation station (44.56°N, 122.92°E, 151 m above mean sea level) was established in the northwest part of Jilin Province, China.

Aerosol is a potential climate change agent, but with a low level of scientific understanding because of the highly spatial and temporal variability in its physical/chemical properties and large uncertainties in its radiative forcing (IPCC, 2013). Dust aerosols from arid and semi-arid regions are the main sources of dust in Asia, and significantly impact regional climate via direct radiative forcing, indirect and semi-direct effects on cloud generation, evolution and dissipation (Huang et al., 2006, 2010). Short-term observation of near-surface $PM_{2.5}$ particles, including their chemical composition and optical properties, has been conducted at Tongyu during spring (Zhang et al., 2008, 2012a; Ho et al., 2011; Shen et al., 2011; Wu et al., 2012). Results from these previous studies clearly indicated that, even in the dusty season, anthropogenic aerosol components such as water-soluble ions, black carbon (BC), and organic carbon accounted for a large portion of aerosol loading. This mixture of natural dust and anthropogenic aerosols had a complex impact on radiation and regional climate change (Che et al., 2009a). Extensive long-term observations of physical/optical parameters including aerosol optical depth (AOD), particle size and absorption have been rarely reported in the literature.

Ground-based remote sensing by sun photometry has been validated as a good method to study column-integrated aerosol optical properties in the atmosphere (Dubovik et al., 2000). Such datasets are widely used to study aerosol radiative forcing and its climate effect (e.g., Xia et al., 2007a, 2007b; Che et al., 2014), and to validate satellite remote sensing (e.g., Hsu et al., 1999; Remer et al., 2002; Bréon et al., 2011; Xie et al., 2011) and chemical model simulation results (e.g., Chin et al., 2002; Matthias, 2008; Han et al., 2012). Regional and global networks, such as the China Aerosol Remote Sensing Network (CARSNET) (Che et al., 2009b), and the Aerosol Robotic Network (AERONET) (Holben et al., 1998), have been established in recent decades. The aerosol optical properties revealed by these networks have been intensively reported over certain regions in China, such as the North China Plain (Xia et al., 2007a; Li et al., 2007; Zhu et al., 2014), eastern China (Xia et al., 2007b; Pan et al., 2010) and western desert regions (Xia et al., 2004; Che et al., 2009a). However, similar studies are very limited in Northeast China, especially in the climatically important semi-arid region. Aerosol optical properties, and related radiative effects in a suburban region, northeastern China (Liaozhong), were studied by Xia et al. (2007c) using sun photometer observations over three months. The spatiotemporal variation of AOD and the Ångström exponent (AE) was described by Wang et al. (2010) with four years of sun photometer measurements at a regional background site in Northeast China (Longfengshan); Zhao et al. (2013) also used sun photometer measurements at four stations over urban and industrial regions of Northeast China to conduct similar studies. However, only selected optical parameters, such as AOD, have been analyzed in this region; detailed analysis of aerosol size and absorption, which have decisive impact on radiative forcing, has not taken place.

In this study, the column-integrated aerosol optical properties at Tongyu are investigated based on four years of sun photometer remote sensing measurements. The optical and microphysical properties including the AOD, single scattering albedo (SSA), absorption AOD (AAOD), and volume size distribution, are analyzed in detail. The aerosol direct radiative forcing (ADRF) is also discussed. This work is intended to give a sense of the columnar aerosol optical properties in a typical semi-arid region in Northeast China, and provide essential parameters to increase the accuracy of climate simulations in this sensitive region.

2. Measurements and methods

2.1. Site description

The Tongyu observation station, a typical semi-arid site in Northeastern China, is a reference site of the Coordinated Energy and Water Cycle Observation Project (CEOP), part of the Global Energy and Water Cycle Exchanges Project (GEWEX). The Tongyu station lies in a degraded grassland area, with very few anthropogenic emission sources (Cheng et al., 2010; Wu et al., 2012). Routine meteorological and water vapor flux measurements have been conducted since October 2002. Long-term continuous observations of aerosol optical parameters began in March 2010, including measurements of near-surface aerosol absorption and scattering coefficients, as well as column-integrated parameters.

From the cluster analysis of the 3-day backward trajectories (HYSPLIT Model, Draxler and Rolph, 2013) ended at the Tongyu observation station (500 m above ground level) during the period from March 2010 to February 2014 (Fig. 1), roughly 20% of air masses arriving at Tongyu came from the heavily polluted south. This region includes the Jing-Jin-Ji area, where the fine-particle pollution was severe. Furthermore, airflows from the west likely transported dust aerosols in spring.

2.2. Measurements

As a regional background site of the China Aerosol Remote Sensing Network (CARSNET), continuous measurements using

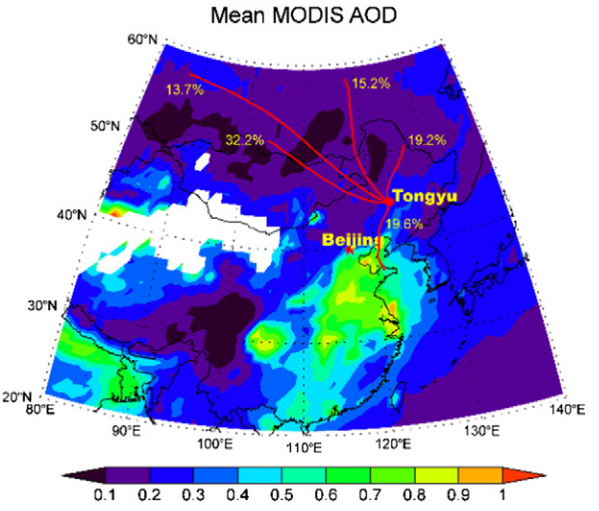

Fig. 1. Spatial distribution of the mean MODIS (aboard NASA's Aqua satellite) AOD at 550 nm from March 2010 to February 2014. The clusters of the 3-day backward trajectories ended at Tongyu (500 m above ground level) are overlaid.

a ground-based sun photometer (CE318, Cimel Electronique, France) were conducted at the Tongyu observation station from March 2010. The sun photometer was situated on the roof of the observation station, ~4 m above the ground. The sun photometer measured direct solar radiance across nine channels from the near-infrared through to the ultraviolet at 1640, 1020, 870, 675, 500, 440, 380, 340 and 940 nm with a 1.2° full field-of-view (Holben et al., 1998). Measurements on the first eight channels were used to retrieve the AOD, with those at 940 nm used to retrieve precipitable water (PW) in the atmosphere. Sky radiances from almucantar scenarios at 440, 675, 870 and 1020 nm were used to retrieve the column-integrated aerosol optical and microphysical parameters such as SSA, refractive index (RI) and volume size distribution (Dubovik and King, 2000; Dubovik et al., 2006).

The sun photometer was calibrated once per year. An inter-comparison calibration was carried out at the Chinese Academy of Meteorological Science (CAMS) using the method described by Che et al. (2009b). The sphere calibration was performed by using the CARSNET sphere that was described in detail in Tao et al. (2014).

2.3. Retrieval methods

AOD was derived using the ASTPwin software provided by the sun photometer manufacturer. Cloud-screening procedures suggested by Smirnov et al. (2000) were applied to eliminate cloud contamination. AOD retrieved from this software agrees well with those of AERONET/PHOTONS based on inter-comparison measurements (Che et al., 2009b). The total uncertainty associated with the AOD is 0.01–0.02 (Eck et al., 1999; Che et al., 2009b). The retrieval algorithm for column-integrated optical properties and radiative forcing of aerosols was similar to that used by AERONET (Che et al., 2014). Column-integrated SSA, RI and size distribution were also retrieved. Note that only the SSA and RI of almucantar retrievals with AOD at 440 nm (AOD_{440}) > 0.4 were retained in this study, to avoid the large inversion errors from the limited information content when AOD_{440} < 0.4 (Dubovik and King, 2000). The retrieval accuracy of SSA is expected to be 0.03 in the high AOD cases. The retrieval errors of aerosol size distribution are <10% in the radius of ~0.7 μm and increase up to 35% with decreasing radius to ~0.1 μm. The uncertainties in retrieved size distribution are relatively large for small particles with radius less than 0.1 μm and particles larger than 0.7 μm (Dubovik et al., 2000; Dubovik and King, 2000; Dubovik et al., 2002).

According to the retrieved parameters, including size distribution, RI and the fraction of spherical particles, the ADRF and its efficiency (i.e., radiative forcing normalized to one unit of AOD) were calculated using a radiative transfer module, as used in the AERONET inversion code (García et al., 2012). The surface albedo, required for calculating the ADRF, was obtained from the 8-day Moderate Resolution Imaging Spectroradiometer (MODIS) land products (MCD43B3, downloaded from ftp://e4ft101.cr.usgs.gov/MOTA/MCD43B3.005). Note that instantaneous ADRF for solar zenith angles of 50–80° is presented in this study.

Four years of data were recorded by the sun photometer, from March 2010 through February 2014, and analyzed in this study. Data were quality controlled by manually excluding extreme outliers through comparison to weather records and near-surface measurements.

3. Results and discussion

3.1. Aerosol optical depth

Averaged over the four-year measurement period at the Tongyu observation station, the mean AOD at 500 nm (AOD_{500}) was 0.20 ± 0.26. The mean AOD at Tongyu was much lower than those measured at urban and suburban regions in China. For instance, the annual mean AOD_{500} in Beijing was approximately 0.88 (Xia et al., 2007a). The annual mean AOD_{500} from September 2004 through September 2005 at Xianghe, a suburban site about 70 km east of Beijing, was 0.82 (Li et al., 2007). Pan et al. (2010) showed that the annual mean AOD_{500} was generally greater than ~0.40 over the Yangtze River Delta region, based on more than one year's measurements at five sites in the region. It was even lower than those at some regional background sites, such as Xinglong (a background site in the North China Plain) where the multi-year average of AOD_{440} was reported as 0.28 (Zhu et al., 2014), and Longfengshan (a background site in Northeast China) where the annual mean AOD_{440} was in the range 0.27–0.39 (Wang et al., 2010). The low AOD implies a regional background characteristic with minimal local human activities. However, the mean AOD at Tongyu was considerably higher than that at the Waliguan observation station, one of the World Meteorological Organization-Global Atmospheric Watch (WMO-GAW) baseline sites, where an average AOD_{500} of 0.14 was reported (Che et al., 2011). The mean AOD_{500} at Tongyu is approximately double the reported values for background continental air masses (~0.1–0.15) (Halthore et al., 1992; Bergin et al., 2000).

AOD showed a pronounced seasonal variation, with maximum values in spring and summer (AOD_{500} ~ 0.33 in May and June), and minima in late autumn and winter (AOD_{500} ~ 0.12 to 0.13 in November through January) (Fig. 2 and Table 1). Similar seasonal variation was observed at many other sites over North China, including Beijing (Eck et al., 2005, 2010; Xia et al., 2006), Xianghe (Li et al., 2007), Shangdianzi (Che et al., 2009c) and

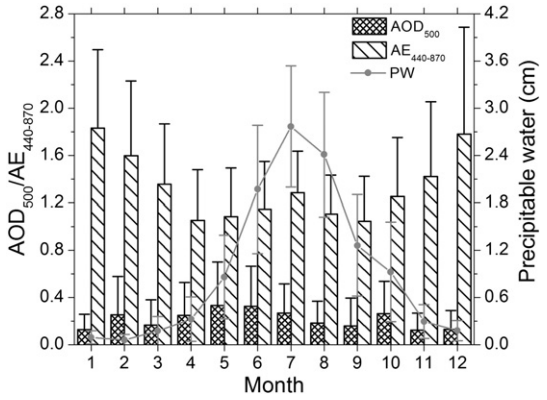

Fig. 2. Monthly variation of AOD at 500 nm, AE between 440 and 870 nm, and the integrated-column PW retrieved from the direct solar radiance measurements by the CE318 sun photometer at Tongyu observation station from March 2010 to February 2014.

Table 1
Seasonal average AOD at 440, 500, 675, 870, and 1020 nm, AE between 440 and 870 nm, and PW at Tongyu observation station from March 2010 to February 2014. Spring: March, April and May; Summer: June, July and August; Autumn: September, October and November; and Winter: December, January and February. *N* is the number of samples.

Season	*N*	AOD_{440}	AOD_{500}	AOD_{675}	AOD_{870}	AOD_{1020}	$AE_{440-870}$	PW (cm)
Spring	8199	0.28 ± 0.31	0.24 ± 0.30	0.19 ± 0.27	0.15 ± 0.26	0.14 ± 0.26	1.17 ± 0.48	0.43 ± 0.45
Summer	5265	0.29 ± 0.30	0.26 ± 0.27	0.18 ± 0.21	0.14 ± 0.16	0.11 ± 0.14	1.17 ± 0.37	2.35 ± 0.85
Autumn	8576	0.20 ± 0.26	0.18 ± 0.23	0.13 ± 0.17	0.09 ± 0.13	0.12 ± 0.18	1.24 ± 0.54	0.83 ± 0.67
Winter	10,100	0.19 ± 0.23	0.16 ± 0.22	0.12 ± 0.18	0.08 ± 0.17	0.08 ± 0.16	1.75 ± 0.76	0.12 ± 0.11
Whole	32,140	0.23 ± 0.28	0.20 ± 0.26	0.15 ± 0.21	0.11 ± 0.19	0.11 ± 0.19	1.37 ± 0.64	0.75 ± 0.93

Xinglong (Zhu et al., 2014) in the North China Plain, and Longfengshan (Wang et al., 2010) in Northeast China. Kim et al. (2007) also demonstrated a similar seasonal variation of AOD over eastern Asia, determined from multi-year MODIS, LIDAR, and AERONET radiometer measurements. The seasonal pattern was also observed in the trans-Himalayan region where airborne dust particles contributed greatly to the higher AOD in spring (Ningombam et al., 2014a). Arid and semi-arid region in East Asia is one of the main sources of eolian dust aerosols in the atmosphere which have great impact on regional and global climates (Choobari et al., 2014). Dust events mostly occurred in spring over East Asia including our study area (Wu et al., 2011). Thus, a higher AOD in spring at this semi-arid site was generally associated with the occasional long-range transportation of dust aerosols upwind from dust source regions, or local dust emissions. The higher AOD in summer was associated with anthropogenic aerosols from stagnant synoptic meteorological patterns, secondary aerosol formation under higher temperatures, increased human activities such as biomass burning, and hygroscopic growth of aerosols due to enhanced relative humidity (the highest PW in summer as shown in Fig. 2). Long-range transportation of anthropogenic aerosols from southern industrial regions also played an important role (Fig. 1 and Fig. S1 in supplementary file). Higher AODs in October (AOD_{500} ~ 0.26) and February (AOD_{500} ~ 0.25) were also observed, perhaps due to the increased anthropogenic emissions from surrounding areas. In situ aethalometer measurements at Tongyu revealed a high BC concentration in October, attributed to increased fuel and biomass burning during harvest (Cheng et al., 2010). The minimum AOD in November through January was representative of the background continental air masses.

The AE of the spectral AOD, an indication of the aerosol size, was calculated by linear regression of AOD against wavelength on a logarithmic scale for all AODs at wavelengths in the range of 440 nm to 870 nm. The annual mean $AE_{440-870}$ was 1.37 ± 0.64 at Tongyu, indicating the dominant contribution of fine-mode particles to aerosol light extinction. The AE also showed a distinct seasonal variation, generally opposite to that of AOD, with higher values during winter and autumn compared to spring and summer. The low AE in spring correlated with occasional dust events in the semi-arid region, which transported or locally produced coarse-mode dust particles. The minimum monthly mean $AE_{440-870}$ at Tongyu was 1.05 in April, suggesting that even during the peak dust month, fine-mode particles dominated the AOD. The $AE_{440-870}$ was lower in summer and early autumn (from June through October), with a mean value in the range of ~1.0 to 1.3. Considering the relatively rare appearance of coarse dust particles during these months, the low AE indicates the occurrence of large size accumulation fine-mode particles, which may have resulted from hygroscopic growth in a humid environment. The mean $AE_{440-870}$ exceeded 1.6 during winter, with a maximum of 1.83 in January, suggesting combustion-produced aerosols which are predominately fine-mode particles accounted mostly for AOD, which is further supported by the analysis of AE and particle size in the next section.

3.2. Aerosol size distribution

The overall mean volume size distribution is shown in Fig. 3 (gray line with vertical error bars). As is typical, the distribution was bimodal, with a fine-mode peak at ~0.15 μm and a coarse-mode peak at ~4 μm. The retrieved size distributions were averaged by season and showed obvious variation (Fig. 3). Generally, the retrieved total volume concentration was highest in spring (0.088 ± 0.109), followed by summer (0.082 ± 0.072) and autumn (0.066 ± 0.075), and lowest in winter (0.051 ± 0.056). Moreover, coarse-mode particles were more abundant in spring, while fine-mode particles were more abundant in summer. The highest fine-mode concentration resulted in the highest AOD in summer. An interesting feature in summer was that the fine-mode effective radius was the largest, indicating coagulation or hygroscopic growth of fine-mode particles, leading to enhanced scattering by aerosols. The contribution of fine- and coarse-mode particles to the total AOD was estimated based on the size distribution retrievals. The AOD_{440} attributable to fine-mode particles accounted for 82%, 92%, 86% and 89% in spring, summer, autumn and winter, respectively, further suggesting the dominant contribution of

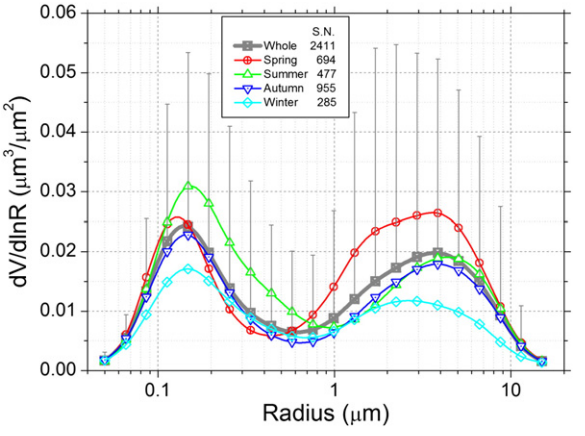

Fig. 3. Seasonal average of aerosol volume size distributions.

fine-mode particles to AOD at Tongyu, revealed by the high AE values.

Although AE is a good indication of particle size, the mixture of coarse- and fine-mode particles makes it ambiguous in some cases. For instance, a fine-mode particle distribution skewed toward larger radii leads to an AE similar to that of a mixture of coarse-mode and smaller fine-mode particles (Gobbi et al., 2007). The relationship between the fine-mode fraction of AOD_{675} (FMF_{675}) and $AE_{440–870}$ is shown in Fig. 4a. When FMF_{675} < ~0.6, there was a positive correlation between FMF and AE, so AE was a good indicator of aerosol size in these cases. However, AE varied widely (~0.0–2.0) for FMF_{675} > ~0.6, indicating that AE was not always related to aerosol size and FMF. This is mostly due to the very large variation of the fine mode radius, as shown in Fig. 4b. There were many cases with fine mode radii larger than 0.2 μm when FMF_{675} > 0.6, indicating that coagulation and hydroscopic growth of aerosols resulted in larger FMF but relatively lower AE. This feature was more obvious in summer, i.e. the rainy season with enhanced humidity.

According to the relationship shown in Fig. 4a, the linear decrease of FMF_{675} with decreasing $AE_{440–870}$ was more significant when FMF_{675} was lower than ~0.6. Therefore, the variation of aerosol size distribution with AOD in two different situations is discussed: one with FMF_{675} > 0.6, representing a fine-mode-dominated situation; and another with FMF_{675} < 0.6, representing a coarse-mode-dominated situation. The average volume size distributions of seven increased AOD bins in the predominantly fine-mode AOD cases (FMF_{675} > 0.6) are shown in Fig. 5a. The volume concentration of the fine mode increased with AOD. Moreover, an obvious increase in the fine-mode radius was observed, similar to those measured at other sites such as Beijing and Anmyon Island, South Korea (Eck et al., 2005). This tendency is likely due to aerosol coagulation or hygroscopic growth. The peak fine-mode radius was relatively smaller than that in Beijing. For example, the peak fine-mode radius in Beijing was ~0.17 μm for an AOD_{440} of 0.68–0.70 (Eck et al., 2005), while it was ~0.14 μm at Tongyu. The smaller fine-mode radius at Tongyu is likely related to its semi-arid environment that suppresses hygroscopic growth. The volume size distributions of coarse-mode-dominated cases are shown in Fig. 5b. The volume concentration increased with AOD, further suggesting a major contribution of coarse-mode particles in these cases. As a result, the AE decreased gradually from ~1.0 to 0.5. The volume median radius of coarse-mode particles was ~2 μm in high AOD cases (e.g., AOD_{440} > 0.7), close to those observed at Beijing and Anmyon Island. This implies a common coarse size characteristic of East Asian dust particles. The fine-mode size associated with the predominantly coarse mode AOD cases showed little dynamic change.

3.3. Single scattering albedo

The average SSA, calculated from 391 almucantar scan retrievals of the four years of measurements for the cases with AOD_{440} > 0.4 was 0.91 ± 0.04 at 440 nm, slightly lower than those at Xianghe and Xinglong in the North China Plain where the mean SSA at 440 nm (SSA_{440}) was ~0.92 (Li et al., 2007; Zhu et al., 2014). Seasonal variation calculated from the limited dataset shows that the mean SSA_{440} was highest in winter (0.920 ± 0.031, 38 retrievals), followed by summer (0.918 ± 0.044, 109 retrievals) and autumn (0.915 ± 0.033, 125 retrievals), and lowest in spring (0.903 ± 0.043, 119 retrievals). Frequent dust releases likely contributed to the lowest SSA_{440} in spring. Dust particles are commonly considered having strong absorption in the range of ultraviolet to short visible light because of the existence of hematite (Fialho et al., 2006 and references therein). It can be approved by the seasonal variation of SSA in the predominantly fine mode cases with FMF_{675} > 0.6. Having excluded the effects of coarse dust particles, the mean SSA_{440} in the predominantly fine mode cases was still highest in winter (0.921 ± 0.037, 34 retrievals), and lowest in autumn (0.917 ± 0.033, 118 retrievals). However, the mean SSA_{440} in spring increased to 0.920 ± 0.034 when 39 coarse-mode retrievals were eliminated. The homologous change in SSA at the other wavelengths was negligible, even in spring, which suggests that the coarse dust particles mainly impacted the SSA at shorter wavelengths (i.e., less than 440 nm). The SSA at longer wavelengths was dominated by fine anthropogenic aerosols, such as BC.

The variation of SSA as a function of AOD is shown in Fig. 6. The mean SSA was calculated in different AOD bins, the same as those described in Subsection 3.2. Predominantly fine- or coarse-mode AOD cases were separated using a critical FMF_{675} larger or less than 0.6. In the fine-mode-dominated cases (FMF_{675} > 0.6), the SSA_{440} increased with increasing AOD_{440},

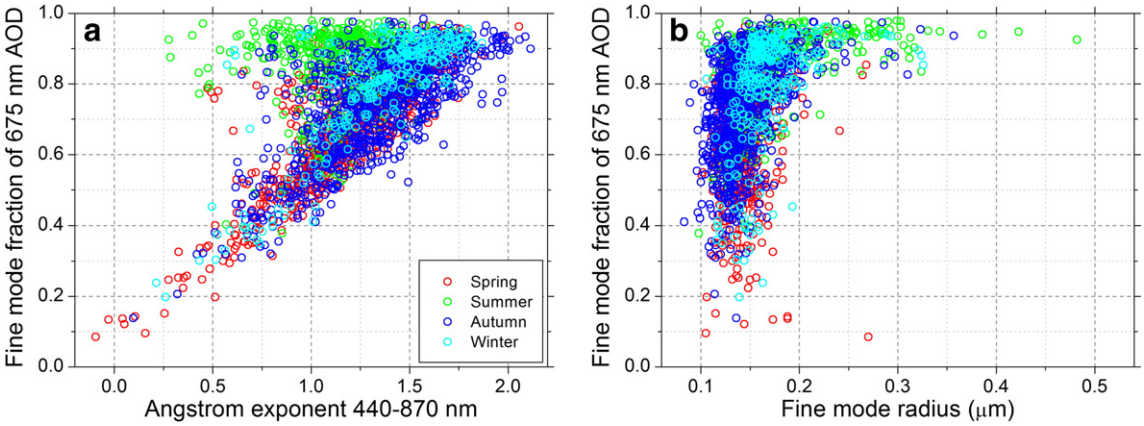

Fig. 4. Scatter-plots of FMF_{675} against (a) $AE_{440–870}$ and (b) as a function of fine-mode radius.

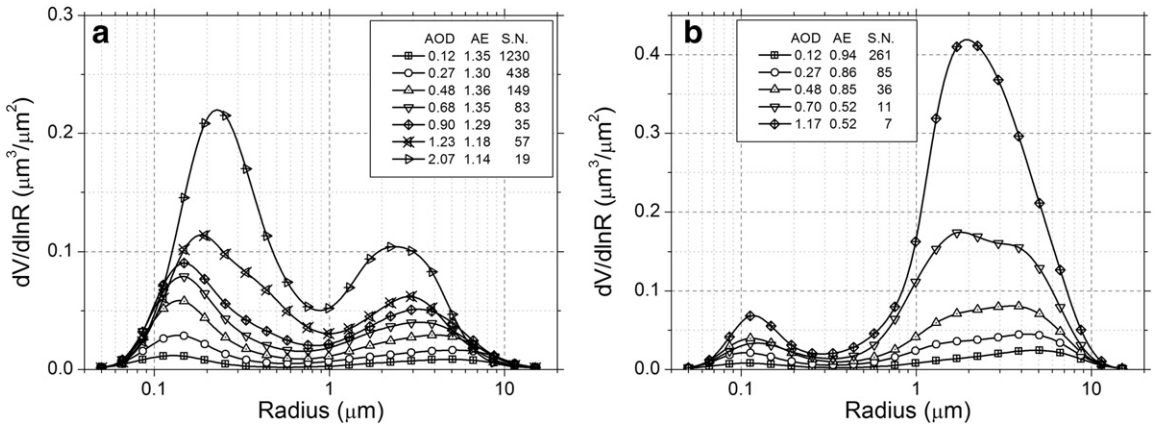

Fig. 5. Aerosol volume size distributions at different AOD_{440} bins in (a) predominantly fine-mode AOD cases with $FMF_{675} > 0.6$, and (b) predominantly coarse-mode cases with $FMF_{675} < 0.6$.

with a minimum of ~0.90 in the lowest AOD bin (mean AOD_{440} ~ 0.48), and maximum of ~0.96 in the highest AOD bin (mean AOD_{440} ~ 2.07). Increases in SSA with AOD were also observed in the predominantly coarse-mode cases ($FMF_{675} < 0.6$), but were less significant at shorter wavelengths (less than 440 nm). The lower SSA_{440} was related to the stronger absorption by dust at this wavelength. The relationship between SSA and AOD at Tongyu suggests that aerosol scattering increased more than absorption as AOD increased, in both the predominantly fine-mode cases (mainly induced by anthropogenic pollution) and the coarse-mode cases (mainly dominated by dust events).

Spectral SSA and volume size distributions for $AOD_{440} > 0.4$ were averaged over nine FMF_{675} bins with ranges of 0–0.2, 0.2–0.3, 0.3–0.4, 0.4–0.5, 0.5–0.6, 0.6–0.7, 0.7–0.8, 0.8–0.9, and 0.9–1.0, as shown in Fig. 7. For the predominantly coarse-mode AOD cases (FMF_{675} = 0.12, 0.25, and 0.36), the SSA generally increased with increasing wavelength, suggesting a stronger wavelength dependence of aerosol absorption compared to scattering (Fig. 7a). A high percentage of coarse-mode particles increased the scattering efficiency at long wavelengths, resulting in weak scattering wavelength dependence (e.g., $AE_{440–870} <$ 0.7). Meanwhile, coarse aerosols have much stronger absorption at shorter wavelengths (in the ultraviolet) due to iron oxides in dust particles, leading to high absorption wavelength dependence in the ultraviolet to near-infrared spectrum range (Fialho et al., 2006; Wu et al., 2012). For approximately equal contributions of fine- and coarse-mode particles to the AOD at 675 nm (FMF_{675} = 0.46, and 0.55), the SSA varied less with wavelength, indicating a comparable wavelength dependence of scattering and absorption. The mean $AE_{440–870}$ was close to 1 in these cases, suggesting a similar absorption Ångström exponent with value near 1 which implies a dominant contribution of BC to particle absorption (Bergstrom et al., 2007). Decreasing SSA with increasing wavelength was observed in the predominantly fine-mode AOD cases ($FMF_{675} > 0.6$) due to the dramatic decrease in scattering efficiency at long wavelengths.

3.4. Absorption aerosol optical depth

The AAOD, as the absorption part of AOD, was calculated from AOD multiplied by (1 − SSA) for the cases with $AOD_{440} > 0.4$. The mean value of AAOD at 440 nm ($AAOD_{440}$) was highest in autumn (0.061 ± 0.023) and lowest in summer (0.055 ± 0.030), with an overall mean of 0.06 ± 0.03. Higher $AAOD_{440}$ was also observed in spring (0.061 ± 0.037), influenced by the coarse dust particles mentioned in Subsection 3.3. Excluding the predominantly coarse-mode cases ($FMF_{675} < 0.6$),

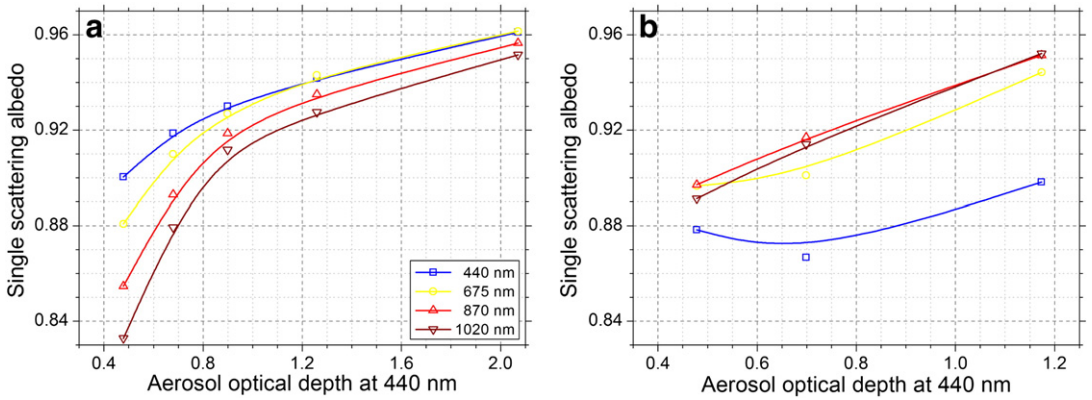

Fig. 6. Variation of SSA as a function of AOD_{440} at four wavelengths when $AOD_{440} > 0.4$ in the (a) predominantly fine-mode cases with $FMF_{675} > 0.6$ and (b) predominantly coarse-mode cases with $FMF_{675} < 0.6$.

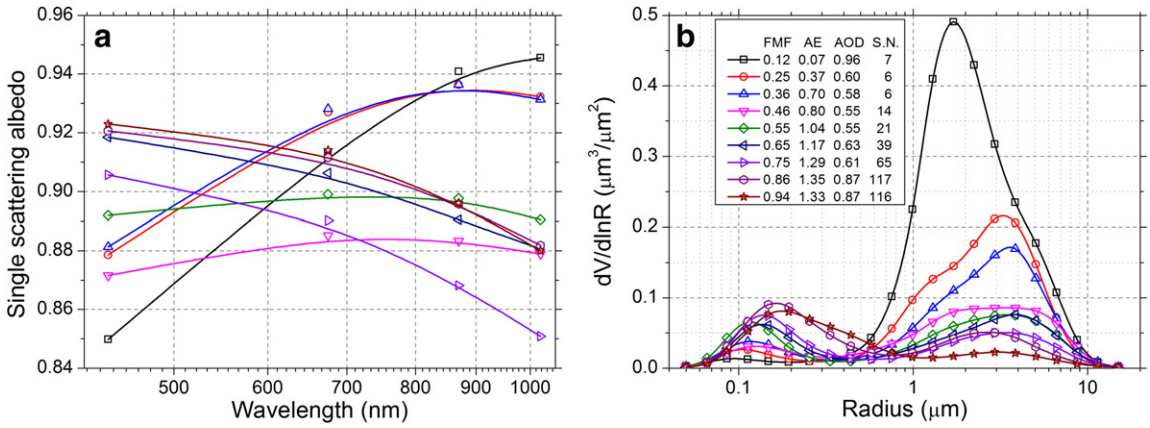

Fig. 7. Almucantar retrievals of (a) spectral SSA and (b) volume size distribution averaged over different FMF_{675} bins when $AOD_{440} > 0.4$.

the mean $AAOD_{440}$ in spring decreased to 0.050 ± 0.027, the lowest among the four seasons. Although the AOD was higher in summer (see Subsection 3.1), the lower AAOD suggests that the aerosol scattering accounted greatly for the higher AOD in summer. By contrast, the effect of the absorbing particles on AOD increased in autumn resulting in the highest AAOD, likely related to increased fuel and biomass burning during harvest (Cheng et al., 2010).

Analogous to AE, the absorption Ångström exponent (AAE) was calculated by replacing AOD with AAOD. The mean $AAE_{440–870}$ at Tongyu was 1.04 ± 0.43, close to the widely adopted value (~1) for BC particles emitted by coal combustion and vehicle exhausts (Bergstrom et al, 2007; Li et al., 2010; Zhang et al., 2012b). The seasonal mean $AAE_{440–870}$ was highest in winter (1.36 ± 0.27) and lowest in summer (0.82 ±0.31). The means for autumn and spring were 1.20 ± 0.29 and 0.96 ± 0.54, respectively. The $AAE_{440–870}$ was higher than 1 in winter and autumn, suggesting that absorption species other than BC have notable impact on aerosol absorption. Having excluded the rare dust cases in winter and autumn, the $AAE_{440–870}$ was still significantly higher than 1, with means of 1.39 ± 0.23 and 1.19 ± 0.29, respectively. This indicates that components such as brown carbon (BrC), which have a larger AAE (Andreae and Gelencsér, 2006) contributed considerably to aerosol absorption. Human activities related to biomass burning in autumn and winter, such as straw burning after harvest and residential heating, are important sources of BrC. In addition to measurement and retrieval uncertainties, the lower $AAE_{440–870}$ in spring and summer may be related to the coating of BC particles by other components, which can lead to an AAE lower than 1 (Bergstrom et al., 2007; Gyawali et al., 2009). Without intense local emission close to the remote site of Tongyu, long-range transportation is likely the major source of anthropogenic aerosols in summer and spring. These bring aged and well-coated BC particles resulting in lower AAE.

3.5. Aerosol direct radiative forcing

Because of the increase in light scattering and absorption induced by aerosol particles, the absolute value of the negative ADRF gradually increased with increasing AOD, both at the bottom of the atmosphere (BOA) and the top of the atmosphere (TOA) (Fig. 8a). The mean ADRF at the BOA varied from around $-20\ W\ m^{-2}$ ($AOD_{440} < 0.2$) to about $-150\ W\ m^{-2}$ ($AOD_{440} > 1.5$). The mean ADRF at the TOA ranged from close to zero to $-70\ W\ m^{-2}$. Similar results over an urban region in northern China were reported by Xia et al. (2007a). Large variation of ADRF was also observed in similar AOD cases (shown by the

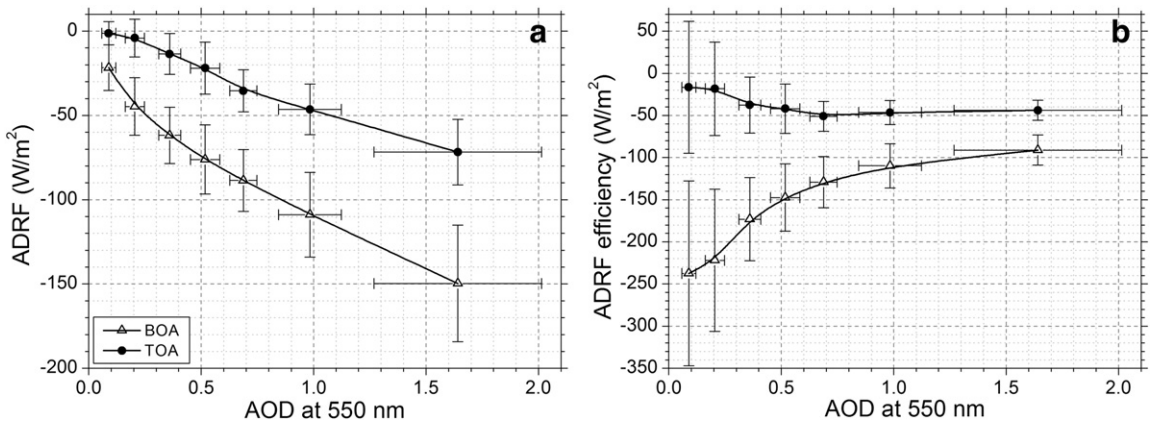

Fig. 8. Variation of (a) ADRF and (b) its efficiency at the BOA and TOA as a function of AOD at 550 nm. The horizontal and vertical error bars represent one standard deviation of the corresponding variable.

large standard deviation of ADRF in each AOD bin in Fig. 8a), suggesting that aerosol properties greatly impact radiation, in addition to aerosol loading. The ADRF efficiency is reflected in the effect of aerosol properties on radiation, expressed as the ADRF normalized by AOD_{550}. Although large deviations existed in the ADRF efficiency when AOD was low, the mean ADRF efficiency (i.e., the absolute value of the negative ADRF efficiency) at the BOA had a significantly decreasing trend as AOD increased, from roughly -240 W m^{-2} in the lowest AOD cases to around -90 W m^{-2} in the highest AOD cases (Fig. 8b). The ADRF efficiency at the TOA varied less with increasing AOD, from -16 W m^{-2} to -50 W m^{-2}. The decrease in ADRF efficiency at the BOA may relate to increases in SSA (i.e., decreasing aerosol absorption) as AOD increased, as mentioned in Subsection 3.3. Greater absorption induces larger ADRF efficiency at the BOA (García et al., 2012). Convergence of the difference between ADRF efficiency at the BOA and TOA with increasing AOD also corroborates the decrease in aerosol absorbing efficiency in the atmosphere as AOD increased.

The mean ADRF, averaged over the retrievals with $AOD_{440} > 0.4$, was -75.17 ± 29.70 W m^{-2} at the BOA and -29.56 ± 19.24 W m^{-2} at the TOA. These values can only represent the pollution conditions at Tongyu where the overall mean AOD_{440} was 0.23. Correspondingly, the mean ADRF efficiency was -139.26 ± 41.57 W m^{-2} and -49.94 ± 21.81 W m^{-2} at the BOA and TOA, respectively. The ADRF efficiency (absolute value) at the BOA is lower than that over the polluted North China Plain where the ADRF efficiency generally exceeded -150 W m^{-2} (Che et al., 2014), suggesting higher SSA (i.e., lower absorption ability) at Tongyu. Compared to the ADRF efficiency at the BOA during typical dust events (~-90 to -110 W m^{-2} reported in Obregón et al., 2015), the value at Tongyu is relatively higher suggesting that more anthropogenic absorption aerosols existed in the atmosphere over the research region. Because of the large uncertainties in retrieved optical properties in low AOD cases (i.e., $AOD_{440} < 0.4$), it was assumed that the optical properties in the cases with $AOD_{440} > 0.4$ were representative of the general characteristics of atmospheric aerosol at Tongyu and estimated the mean ADRF over all the almucantar scan retrievals by multiplying the mean ADRF efficiency by the overall mean AOD_{550}. As a result, the overall mean ADRF at the BOA and TOA was -26.28 and -9.42 W m^{-2} respectively, suggesting a cooling effect of aerosol in this semi-arid region. The difference between ADRFs at the TOA and BOA reflects the ADRF in the atmosphere due to aerosol absorption. The mean ADRF in the atmosphere was ~17 W m^{-2} at Tongyu, high enough to cause heating of the atmosphere and possibly impacting atmospheric stability and the water cycle (Ramanathan et al., 2001; Ningombam et al., 2014b). Analogously, the seasonal ADRFs were estimated, and determined to have means of -30.52, -34.19, -22.44, and -18.94 W m^{-2} in spring, summer, autumn, and winter, respectively, at the BOA; and -9.60, -12.81, -8.03, and -8.78 W m^{-2}, respectively, at the TOA. The lower-level cooling and higher-level heating effect may further have likely impact on the regional climate, e.g. weakening the East Asian monsoon circulation. Thus, it is important to have long-term monitoring of aerosols and their radiative properties in the typical semi-arid region.

4. Summary and conclusions

Column-integrated aerosol optical properties at the Tongyu observation station, a rural site located in the climate-sensitive semi-arid region of Northeast China, were analyzed based on the retrievals of four years of sun photometer measurements from March 2010 to April 2014. The overall average AOD_{500} was 0.20 ± 0.26, approximately a quarter of that observed in the polluted North China Plain and the Yangtze Delta Region. The AOD showed a significant seasonal variation, with higher mean values in summer and spring. The $AE_{440–870}$ was 1.37 ± 0.64 averaged over the whole period, suggesting a dominant contribution of fine-mode particles to the AOD. The AE had a generally opposite seasonal variation pattern. Higher AOD but lower AE in summer might relate to increased transport of anthropogenic aerosol from southern areas, accompanied by hygroscopic particle growth; in spring this could be induced by an increased contribution of coarse dust particles.

Separate relationships between AE and FMF illustrated the different effects of particle sizes on AE. The particle sizes were enhanced by increases in coarse-mode particles, which induced a decrease of AE with decreasing FMF. However, hygroscopic growth resulted in the breakdown of the relationship between AE and FMF. The coarse mode increased significantly as AOD increased, in the predominantly coarse dust cases ($FMF_{675} < 0.6$). These mainly occurred in spring, resulting in a markedly decreased AE. In the fine-mode-dominated cases ($FMF_{675} > 0.6$), the fine mode increased more significantly with increasing AOD accompanied by the increase in fine-mode sizes.

The SSA_{440} averaged over the retrievals with $AOD_{440} > 0.4$ was 0.91 ± 0.05. This parameter also displayed seasonal cycles, with lower values in spring and autumn and maxima in winter. Dust particles in spring played an important role in aerosol absorption at 440 nm. Increases in SSA were observed as AOD increased, indicating that the aerosol scattering increased more than absorption in the increasing AOD cases. Because of the increased scattering efficiency, as well as the decreased absorption efficiency of dust at long wavelengths, the SSA increased with wavelength in the coarse-mode-dominated cases. The SSA decreased with increased wavelength in the fine-mode-dominated cases, suggesting a strong spectral dependence of scattering compared to absorption.

The $AAOD_{440}$ was highest in autumn and lowest in summer, with an overall mean of 0.06 ± 0.03. The mean $AAE_{440–870}$ at Tongyu was 1.04 ± 0.43. It was significantly higher than 1 in winter and autumn, suggesting that BrC contributed considerably to aerosol absorption. The $AAE_{440–870}$ was lower than 1 in summer and spring, related to the coating of BC particles.

A cooling effect of aerosol was found at Tongyu, with a mean ADRF of -26.28 W m^{-2} at the BOA, and -9.42 W m^{-2} at the TOA. The negative ADRF showed a gradual increase as AOD increased because of the increased aerosol loading in the atmosphere. However, regardless of aerosol loading at the BOA, the ADRF efficiency decreased as AOD increased, suggesting a decreased aerosol absorbing ability. Larger negative ADRF at the BOA and lower ADRF at the TOA may result in a strong cooling effect at the surface, but heating in the body of the atmosphere. This could further impact the regional climate which needs continued work.

Acknowledgments

This work was supported by the National Natural Science Foundation of China (No. 41305128), and the National Basic Research Program of China (No. 2012CB955303). The authors gratefully acknowledge the NOAA Air Resources Laboratory (ARL) for the provision of the HYSPLIT transport and dispersion model and the READY website (http://www.ready.noaa.gov) used in this publication.

Appendix A. Supplementary data

Supplementary data to this article can be found online at http://dx.doi.org/10.1016/j.atmosres.2015.01.021.

References

Andreae, M.O., Gelencsér, A., 2006. Black carbon or brown carbon? The nature of light-absorbing carbonaceous aerosols. Atmos. Chem. Phys. 6, 3131–3148. http://dx.doi.org/10.5194/acp-6-3131-2006.

Bergin, M.H., Schwartz, S.E., Halthore, R.N., Ogren, J.A., Hlavka, D.L., 2000. Comparison of aerosol optical depth inferred from surface measurements with that determined by Sun photometry for cloud-free conditions at a continental U.S. site. J. Geophys. Res. 105 (D5), 6807–6816. http://dx.doi.org/10.1029/1999JD900454.

Bergstrom, R.W., Pilewskie, P., Russell, P.B., Redemann, J., Bond, T.C., Quinn, P.K., Sierau, B., 2007. Spectral absorption properties of atmospheric aerosols. Atmos. Chem. Phys. 7, 5937–5943. http://dx.doi.org/10.5194/acp-7-5937-2007.

Bréon, F.-M., Vermeulen, A., Descloitres, J., 2011. An evaluation of satellite aerosol products against sunphotometer measurements. Remote Sens. Environ. 115 (12), 3102–3111. http://dx.doi.org/10.1016/j.rse.2011.06.017.

Che, H., Zhang, X., Alfraro, S., Chatenet, B., Gomns, L., Zhao, J., 2009a. Aerosol optical properties and its radiative forcing over Yulin, China in 2001 and 2002. Adv. Atmos. Sci. 26 (3), 564–576. http://dx.doi.org/10.1007/s00376-009-0564-4.

Che, H., Yang, Z., Zhang, X., Zhu, C., Ma, Q., Zhou, H., Wang, P., 2009b. Study on the aerosol optical properties and their relationship with aerosol chemical compositions over three regional background stations in China. Atmos. Environ. 43, 1093–1099. http://dx.doi.org/10.1016/j.atmosenv.2008.11.010.

Che, H., Zhang, X., Chen, H., Damiri, B., Goloub, P., Li, Z., Zhang, X., Wei, Y., Zhou, H., Dong, F., Li, D., Zhou, T., 2009c. Instrument calibration and aerosol optical depth validation of the China Aerosol Remote Sensing Network. J. Geophys. Res. 114, D03206. http://dx.doi.org/10.1029/2008JD011030.

Che, H., Wang, Y., Sun, J., 2011. Aerosol optical properties at Mt. Waliguan Observatory. China Atmos. Environ. 45, 6004–6009. http://dx.doi.org/10.1016/j.atmosenv.2011.07.050.

Che, H., Xia, X., Zhu, J., Li, Z., Dubovik, O., Holben, B., Goloub, P., Chen, H., Estelles, V., Cuevas-Agulló, E., Blarel, L., Wang, H., Zhao, H., Zhang, X., Wang, Y., Sun, J., Tao, R., Zhang, X., Shi, G., 2014. Column aerosol optical properties and aerosol radiative forcing during a serious haze–fog month over North China Plain in 2013 based on ground-based sunphotometer measurements. Atmos. Chem. Phys. 14, 2125–2138. http://dx.doi.org/10.5194/acp-14-2125-2014.

Cheng, T., Han, Z., Zhang, R., Du, H., Jia, X., Wang, J., Yao, J., 2010. Black carbon in a continental semi-arid area of Northeast China and its possible sources of fire emission. J. Geophys. Res. 115, D23204. http://dx.doi.org/10.1029/2009JD013523.

Chin, M., Ginoux, P., Kinne, S., Torres, O., Holben, B.N., Duncan, B.N., Martin, R.V., Logan, J.A., Higurashi, A., Nakajima, T., 2002. Tropospheric aerosol optical thickness from the GOCART model and comparisons with satellite and sun photometer measurements. J. Atmos. Sci. 59 (3), 461–483. http://dx.doi.org/10.1175/1520-0469(2002)059<0461:TAOTFT>2.0.CO;2.

Choobari, O.A., Zawar-Reza, P., Sturman, A., 2014. The global distribution of mineral dust and its impacts on the climate system: a review. Atmos. Res. 138, 152–165. http://dx.doi.org/10.1016/j.atmosres.2013.11.007.

Draxler, R.R., Rolph, G.D., 2013. HYSPLIT (HYbrid Single-Particle Lagrangian Integrated Trajectory) Model access via NOAA ARL READY Website (http://www.arl.noaa.gov/HYSPLIT.php). NOAA Air Resources Laboratory, College Park, MD.

Dubovik, O., King, M.D., 2000. A flexible inversion algorithm for retrieval of aerosol optical properties from Sun and sky radiance measurements. J. Geophys. Res. 105 (D16), 20673–20696. http://dx.doi.org/10.1029/2000JD900282.

Dubovik, O., Smirnov, A., Holben, B.N., King, M.D., Kaufman, Y.J., Eck, T.F., Slutsker, I., 2000. Accuracy assessments of aerosol optical properties retrieved from Aerosol Robotic Network (AERONET) Sun and sky radiance measurements. J. Geophys. Res. 105 (D8), 9791–9806. http://dx.doi.org/10.1029/2000JD900040.

Dubovik, O., Holben, B., Eck, T.F., Smirnov, A., Kaufman, Y.J., King, M.D., Tanre, D., Slutsker, I., 2002. Variability of absorption and optical properties of key aerosol types observed in worldwide locations. J. Atmos. Sci. 59, 590–608. http://dx.doi.org/10.1175/1520-0469(2002)059<0590:VOAAOP>2.0.CO;2.

Dubovik, O., Sinyuk, A., Lapyonok, T., Holben, B.N., Mishchenko, M., Yang, P., Eck, T.F., Volten, H., Muñoz, O., Veihelmann, B., van der Zande, W.J., Leon, J.-F., Sorokin, M., Slutsker, I., 2006. Application of spheroid models to account for aerosol particle nonsphericity in remote sensing of desert dust. J. Geophys. Res. 111, D11208. http://dx.doi.org/10.1029/2005JD006619.

Eck, T.F., Holben, B.N., Reid, J.S., Dubovik, O., Smirnov, A., O'Neill, N.T., Slutsker, I., Kinne, S., 1999. Wavelength dependence of the optical depth of biomass burning, urban, and desert dust aerosols. J. Geophys. Res. 104 (D24), 31333–31349. http://dx.doi.org/10.1029/1999JD900923.

Eck, T.F., Holben, B.N., Dubovik, O., Smirnov, A., Goloub, P., Chen, H.B., Chatenet, B., Gomes, L., Zhang, X.-Y., Tsay, S.-C., Ji, Q., Giles, D., Slutsker, I., 2005. Columnar aerosol optical properties at AERONET sites in central eastern Asia and aerosol transport to the tropical mid-Pacific. J. Geophys. Res. 110, D06202. http://dx.doi.org/10.1029/2004JD005274.

Eck, T.F., Holben, B.N., Sinyuk, A., Pinker, R.T., Goloub, P., Chen, H., Chatenet, B., Li, Z., Singh, R.P., Tripathi, S.N., Reid, J.S., Giles, D.M., Dubovik, O., O'Neill, N.T., Smirnov, A., Wang, P., Xia, X., 2010. Climatological aspects of the optical properties of fine/coarse mode aerosol mixtures. J. Geophys. Res. 115, D19205. http://dx.doi.org/10.1029/2010JD014002.

Fialho, P., Freitas, M.C., Barata, F., Vieira, B., Hansen, A.D.A., Honrath, R.E., 2006. The Aethalometer calibration and determination of iron concentration in dust aerosols. J. Aerosol Sci. 37, 1497–1506. http://dx.doi.org/10.1016/j.jaerosci.2006.03.002.

Fu, C., An, Z., 2002. Study of aridification in northern China — a global change issue forcing directly the demand of nation. Earth Sci. Front. 9, 271–275 (in Chinese).

Fu, C., Wen, G., 2002. Several issues on aridification in the northern China. Clim. Environ. Res. 7, 22–29 (in Chinese).

García, O.E., Díaz, J.P., Expósito, F.J., Díaz, A.M., Dubovik, O., Derimian, Y., 2012. Aerosol radiative forcing: AERONET based estimates. In: Druyan, L. (Ed.), Climate Models. InTech. ISBN: 978-953-51-0135-2 http://dx.doi.org/10.5772/32287.

Gobbi, G.P., Kaufman, Y.J., Koren, I., Eck, T.F., 2007. Classification of aerosol properties derived from AERONET direct sun data. Atmos. Chem. Phys. 7, 453–458. http://dx.doi.org/10.5194/acp-7-453-2007.

Gyawali, M., Arnott, W.P., Lewis, K., Moosmüller, H., 2009. In situ aerosol optics in Reno, NV, USA during and after the summer 2008 California wildfires and the influence of absorbing and non-absorbing organic coatings on spectral light absorption. Atmos. Chem. Phys. 9, 8007–8015. http://dx.doi.org/10.5194/acp-9-8007-2009.

Halthore, R.N., Markham, B.L., Ferrare, R.A., Aro, T.O., 1992. Aerosol optical properties over the midcontinental United States. J. Geophys. Res. 97 (D17), 18769–18778. http://dx.doi.org/10.1029/92JD01088.

Han, Z., Li, J., Xia, X., Zhang, R., 2012. Investigation of direct radiative effects of aerosols in dust storm season over East Asia with an online coupled regional climate-chemistry–aerosol model. Atmos. Environ. 54, 688–699. http://dx.doi.org/10.1016/j.atmosenv.2012.01.041.

Ho, K.F., Zhang, R.J., Lee, S.C., Ho, S.S.H., Liu, S.X., Fung, K., Cao, J.J., Shen, Z.X., Xu, H.M., 2011. Characteristics of carbonate carbon in $PM_{2.5}$ in a typical semi-arid area of northeastern China. Atmos. Environ. 45, 1268–1274. http://dx.doi.org/10.1016/j.atmosenv.2010.12.007.

Holben, B.N., Eck, T.F., Slutsker, I., Tanré, D., Buis, J.P., Setzer, A., Vermote, E., Reagan, J.A., Kaufman, Y.J., Nakajima, T., Lavenu, F., Jankowiak, I., Smirnov, A., 1998. AERONET — a federated instrument network and data archive for aerosol characterization. Remote Sens. Environ. 66 (1), 1–16. http://dx.doi.org/10.1016/S0034-4257(98)00031-5.

Hsu, N.C., Herman, J.R., Torres, O., Holben, B.N., Tanre, D., Eck, T.F., Smirnov, A., Chatenet, B., Lavenu, F., 1999. Comparisons of the TOMS aerosol index with Sun-photometer aerosol optical thickness: results and applications. J. Geophys. Res. 104 (D6), 6269–6279. http://dx.doi.org/10.1029/1998JD200086.

Huang, J., Lin, B., Minnis, P., Wang, T., Wang, X., Hu, Y., Yi, Y., Ayers, J.K., 2006. Satellite-based assessment of possible dust aerosol semi-direct effect on cloud water path over East Asia. Geophys. Res. Lett. 33, L19802. http://dx.doi.org/10.1029/2006GL026561.

Huang, J., Zhang, W., Zuo, J., Bi, J., Shi, J., Wang, X., Chang, Z., Huang, Z., Yang, S., Zhang, B., Wang, G., Feng, G., Yuan, J., Zhang, L., Zuo, H., Wang, S., Fu, C., Chou, J., 2008. An overview of the semi-arid climate and environment

research observatory over the Loess Plateau. Adv. Atmos. Sci. 25 (6), 906–921. http://dx.doi.org/10.1007/s00376-008-0906-7.
Huang, J., Minnis, P., Yan, H., Yi, Y., Chen, B., Zhang, L., Ayers, J.K., 2010. Dust aerosol effect on semi-arid climate over Northwest China detected from A-Train satellite measurements. Atmos. Chem. Phys. 10, 6863–6872. http://dx.doi.org/10.5194/acp-10-6863-2010.
IPCC, 2013. Summary for policymakers. In: Stocker, T.F., Qin, D., Plattner, G.-K., Tignor, M., Allen, S.K., Boschung, J., Nauels, A., Xia, Y., Bex, V., Midgley, P.M. (Eds.), Climate Change 2013: The Physical Science Basis. Contribution of Working Group I to the Fifth Assessment Report of the Intergovernmental Panel on Climate Change. Cambridge University Press, Cambridge, United Kingdom and New York, NY, USA.
Kim, S.-W., Yoon, S.-C., Kim, J., Kim, S.-Y., 2007. Seasonal and monthly variations of columnar aerosol optical properties over east Asia determined from multi-year MODIS, LIDAR, and AERONET Sun/sky radiometer measurements. Atmos. Environ. 41, 1634–1651. http://dx.doi.org/10.1016/j.atmosenv.2006.10.044.
Li, Z., Xia, X., Cribb, M., Mi, W., Holben, B., Wang, P., Chen, H., Tsay, S.-C., Eck, T.F., Zhao, F., Dutton, E.G., Dickerson, R.E., 2007. Aerosol optical properties and their radiative effects in northern China. J. Geophys. Res. 112, D22S01. http://dx.doi.org/10.1029/2006JD007382.
Li, W.J., Shao, L.Y., Buseck, P.R., 2010. Haze types in Beijing and the influence of agricultural biomass burning. Atmos. Chem. Phys. 10, 8119–8130. http://dx.doi.org/10.5194/acp-10-8119-2010.
Liu, H., Wang, B., Fu, C., 2008. Relationships between surface albedo, soil thermal parameters and soil moisture in the semi-arid area of Tongyu, northeastern China. Adv. Atmos. Sci. 25 (5), 757–764. http://dx.doi.org/10.1007/s00376-008-0757-2.
Matthias, V., 2008. The aerosol distribution in Europe derived with the Community Multiscale Air Quality (CMAQ) model: comparison to near surface in situ and sunphotometer measurements. Atmos. Chem. Phys. 8, 5077–5097. http://dx.doi.org/10.5194/acp-8-5077-2008.
Ningombam, S.S., Bagare, S.P., Sinha, N., Singh, R.B., Srivastava, A.K., Larson, E., Kanawade, V.P., 2014a. Characterization of aerosol optical properties over the high-altitude station Hanle, in the trans-Himalayan region. Atmos. Res. 138, 308–323. http://dx.doi.org/10.1016/j.atmosres.2013.11.025.
Ningombam, S.S., Bagare, S.P., Srivastava, A.K., Sohn, B.J., Song, H.-J., Larson, E., 2014b. Aerosol radiative forcing over a high-altitude station Merak, in the trans-Himalayan region during advection of anthropogenic events from the Indo-Gangetic Plain. Atmos. Environ. 98, 253–259. http://dx.doi.org/10.1016/j.atmosenv.2014.08.061.
Obregón, M.A., Pereira, S., Salgueiro, V., Costa, M.J., Silva, A.M., Serrano, A., Bortoli, D., 2015. Aerosol radiative effects during two desert dust events in August 2012 over the Southwestern Iberian Peninsula. Atmos. Res. 153, 404–415. http://dx.doi.org/10.1016/j.atmores.2014.10.007.
Pan, L., Che, H., Geng, F., Xia, X., Wang, Y., Zhu, C., Chen, M., Gao, W., Guo, J., 2010. Aerosol optical properties based on ground measurements over the Chinese Yangtze Delta Region. Atmos. Environ. 44, 2587–2596. http://dx.doi.org/10.1016/j.atmosenv.2010.04.013.
Ramanathan, V., Crutzen, P.J., Kiehl, J.T., Rosenfeld, D., 2001. Aerosols, climate, and the hydrological cycle. Science 294, 2119–2124. http://dx.doi.org/10.1126/science.1064034.
Remer, L.A., Tanré, D., Kaufman, Y.J., Ichoku, C., Mattoo, S., Levy, R., Chu, D.A., Holben, B., Dubovik, O., Smirnov, A., Martins, J.V., Li, R.-R., Ahmad, Z., 2002. Validation of MODIS aerosol retrieval over ocean. Geophys. Res. Lett. 29 (12). http://dx.doi.org/10.1029/2001GL013204 (MOD3-1-MOD3-4).
Shen, Z., Wang, X., Zhang, R., Ho, K.F., Cao, J., Zhang, M., 2011. Chemical composition of water-soluble ions and carbonate estimation in spring aerosol at a semi-arid site of Tongyu, China. Aerosol Air Qual. Res. 10, 360–368. http://dx.doi.org/10.4209/aaqr.2011.02.0010.
Smirnov, A., Holben, B.N., Eck, T.F., Dubovik, O., Slutsker, I., 2000. Cloud-screening and quality control algorithms for the AERONET database. Remote Sens. Environ. 73 (3), 337–349. http://dx.doi.org/10.1016/S0034-4257(00)00109-7.
Tao, R., Che, H.Z., Chen, Q.L., Wang, Y.Q., Sun, J.Y., Zhang, X.C., Lu, S., Guo, J.P., Wang, H., Zhang, X.Y., 2014. Development of an integrating sphere calibration method for Cimel sunphotometers in China aerosol remote sensing network. Particuology 13, 88–89. http://dx.doi.org/10.1016/j.partic.2013.04.009.
Wang, P., Che, H., Zhang, X., Song, Q., Wang, Y., Zhang, Z., Dai, X., Yu, D., 2010. Aerosol optical properties of regional background atmosphere in Northeast China. Atmos. Environ. 44, 4404–4412. http://dx.doi.org/10.1016/j.atmosenv.2010.07.043.
Wu, Y.F., Zhang, R.J., Fu, C.B., Gao, Z.T., 2011. Variability of blowing dust weather frequency over semi-arid areas of China (Baicheng, Jilin Province) and relationships with climatic factors during 1951–2006. Terr. Atmos. Ocean. Sci. 22 (3), 315–324. http://dx.doi.org/10.3319/TAO.2010.0915.01(A).
Wu, Y., Zhang, R., Pu, Y., Zhang, L., Ho, K.F., Fu, C., 2012. Aerosol optical properties observed at a semi-arid rural site in northeastern China. Aerosol Air Qual. Res. 12, 503–514. http://dx.doi.org/10.4209/aaqr.2011.11.0202.
Xia, X., Chen, H., Wang, P., 2004. Aerosol properties in a Chinese semiarid region. Atmos. Environ. 38, 4571–4581. http://dx.doi.org/10.1016/j.atmosenv.2004.04.015.
Xia, X., Chen, H., Wang, P., Zhang, W., Goloub, P., Chatenet, B., Eck, T.F., Holben, B.N., 2006. Variation of column-integrated aerosol properties in a Chinese urban region. J. Geophys. Res. 111, D05204. http://dx.doi.org/10.1029/2005JD006203.
Xia, X., Chen, H., Goloub, P., Zhang, W., Chatenet, B., Wang, P., 2007a. A compilation of aerosol optical properties and calculation of direct radiative forcing over an urban region in northern China. J. Geophys. Res. 112, D12203. http://dx.doi.org/10.1029/2006JD008119.
Xia, X., Li, Z., Holben, B., Wang, P., Eck, T., Chen, H., Cribb, M., Zhao, Y., 2007b. Aerosol optical properties and radiative effects in the Yangtze Delta region of China. J. Geophys. Res. 112, D22S12. http://dx.doi.org/10.1029/2007JD008859.
Xia, X., Chen, H., Li, Z., Wang, P., Wang, J., 2007c. Significant reduction of surface solar irradiance induced by aerosols in a suburban region in northeastern China. J. Geophys. Res. 112, D22S02. http://dx.doi.org/10.1029/2006JD007562.
Xie, Y., Zhang, Y., Xiong, X., Qu, J.J., Che, H., 2011. Validation of MODIS aerosol optical depth product over China using CARSNET measurements. Atmos. Environ. 45, 5970–5978. http://dx.doi.org/10.1016/j.atmosenv.2011.08.002.
Zhang, R., Fu, C., Han, Z., Zhu, C., 2008. Characteristics of elemental composition of $PM_{2.5}$ in the spring period at Tongyu in the semi-arid region of Northeast China. Adv. Atmos. Sci. 25 (6), 922–931. http://dx.doi.org/10.1007/s00376-008-0922-7.
Zhang, R., Tao, J., Ho, K.F., Shen, Z., Wang, G., Cao, J., Liu, S., Zhang, L., Lee, S.C., 2012a. Characterization of atmospheric organic and elemental carbon of $PM_{2.5}$ in a typical semi-arid area of northeastern China. Aerosol Air Qual. Res. 12, 792–802. http://dx.doi.org/10.4209/aaqr.2011.07.0110.
Zhang, X.Y., Wang, Y.Q., Niu, T., Zhang, X.C., Gong, S.L., Zhang, Y.M., Sun, J.Y., 2012b. Atmospheric aerosol compositions in China: spatial/temporal variability, chemical signature, regional haze distribution and comparisons with global aerosols. Atmos. Chem. Phys. 12, 779–799. http://dx.doi.org/10.5194/acp-12-779-2012.
Zhao, H., Che, H., Zhang, X., Ma, Y., Wang, Y., Wang, X., Liu, C., Che, H., 2013. Aerosol optical properties over urban and industrial region of Northeast China by using ground-based sun-photometer measurement. Atmos. Environ. 75, 270–278. http://dx.doi.org/10.1016/j.atmosenv.2013.04.048.
Zhu, J., Che, H., Xia, X., Chen, H., Goloub, P., Zhang, W., 2014. Column-integrated aerosol optical and physical properties at a regional background atmosphere in North China Plain. Atmos. Environ. 84, 54–64. http://dx.doi.org/10.1016/j.atmosenv.2013.11.019.